Transition to turbulence in a heated non-Newtonian pipe flow

Francesco Romanò,[1,a)] Antoine Charles,[2] François Dottori,[2] and S. Amir Bahrani[2,b)]

AFFILIATIONS

[1]Univ. Lille, CNRS, ONERA, Arts et Métiers Institute of Technology, Centrale Lille, FRE 2017-LMFL-Laboratoire de Mécanique des Fluides de Lille-Kampé de Fériet, F-59000 Lille, France

[2]IMT Nord Europe, Institut Mines Télécom, Univ. Lille, Center for Energy and Environment, F-59000 Lille, France

[a)]**Author to whom correspondence should be addressed:** francesco.romano@ensam.eu
[b)]**Electronic mail:** amir.bahrani@imt-nord-europe.fr

ABSTRACT

A simplified mono-dimensional model for investigating the transition to turbulence in nonisothermal and non-Newtonian pipe flows is proposed. The flow stability is analyzed within the framework of such a model, showing that uniformly heating the pipe wall leads to an earlier transition to turbulence, while differentially heating the pipe wall produces a stabilizing effect. For power-law fluids, we also demonstrate that an increase in the power-law index, i.e., passing from shear-thinning to shear-thickening fluids, leads to a stabilization of the system.

The transition to turbulence is among the most investigated topics in fluid mechanics as it relies on a number of complex mechanisms not yet fully understood. Several studies focused on linear instabilities triggering the most dangerous perturbations that lead to laminar-to-turbulent transition in model flows such as the Kolmogorov flow[1] or in paradigmatic setups such as the Taylor–Couette[2] or the Rayleigh–Benard flows.[3]

On the other hand, when dealing with pipe flows, nonlinear interactions between finite-amplitude perturbations are essential for transition to turbulence[4,5] as the Hagen–Poiseuille flow is linearly stable. Among the most interesting features of transition to turbulence in pipe flows, there is the phenomenon of intermittent turbulence, where small turbulent regions (*puffs*) grow up to larger turbulent patches (*slugs*), and then they decay because of a restabilization of the mean velocity profile. This has recently been investigated by Barkley,[6] who proposed a reduced-order model that retains only a part of the nonlinear physics in the momentum equation that is essential to explain the intermittency as well as the nonlinear interaction between turbulent and laminar regions leading to transition.

Consistently with the experimental observations, the model proposed by Barkley assumes the existence of a bi-stable flow state, i.e., laminar and turbulent flow states coexist. Potentially, this gives rise to the intermittency phenomena reproduced by a mono-dimensional Partial Differential Equation (PDE) model that couples the intensity of turbulence q and the axial velocity of the flow perturbation u advected by the background flow velocity U. At the core of this interaction, Barkley introduced a power-four polynomial potential term $V(q)$ that admits, in general, three stationary points. When only one of them is real, the potential has only one minimum that corresponds to perturbations decaying to the laminar state q^0. On the other hand, when the $V(q)$ admits three real stationary points, two of them are minima, i.e., linearly stable attractors of the system (q^0 and q^+), and one of them is a maximum, i.e., a linearly unstable repellor of the system (q^-, see Fig. 1). Within the framework of Barkley's model, the normalized Reynolds number $\mathcal{R}$ controls the qualitative shape of the $V(q)$, hence the dynamics of the system (see Barkley *et al.*[7] for details about the relation between the nominal and the normalized Reynolds number). Let us consider the dynamics of a perturbation in the $(q, \mathcal{R})-$ phase diagram. For $\mathcal{R} < 0$, the laminar state is a global attractor of the system, and the turbulent perturbations will unconditionally decay, i.e., q^0 is a globally stable attractor for all the possible perturbations (see blue marker in Fig. 1). For $0 < \mathcal{R} < 1$, the laminar state reduces to a local attractor of the system that coexists with a second attractor created in the turbulent regime (see red marker in Fig. 1). Upon an increase in $\mathcal{R}$, i.e., for $\mathcal{R} > 1$, the local attractor of the turbulent state becomes dominant leading to a shrinkage of the manifold of attraction of the laminar state. Such a simplified picture has been extensively validated against experiments (see Barkley *et al.*[7]) and has provided novel insights in the intricate dynamics of transition to turbulence in pipe flow (see the perspective paper of Barkley[8] for a comprehensive

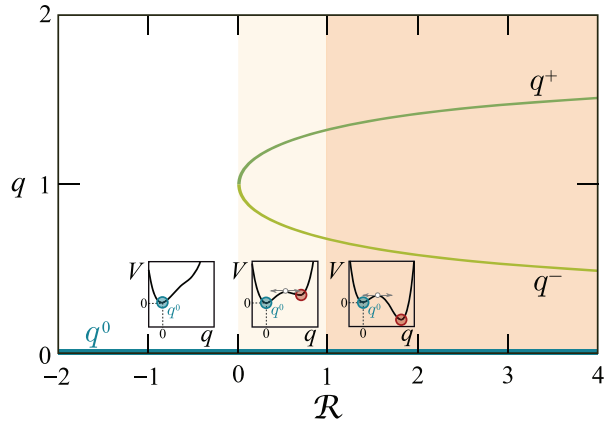

FIG. 1. Phase diagram in terms of the intensity of the turbulence q and of the normalized Reynolds number $\mathcal{R}$. The two green lines show the trace of one of the linearly stable minima of the potential q^+ and of the linearly unstable maximum of the potential q^-, while q^0 denotes the second linearly stable minimum of the potential that corresponds to laminar state, i.e., to the Hagen–Poiseuille flow. The three insets show three representative configurations of the potential term $V(q)$ depending on the normalized Reynolds number. The blue markers denote the laminar state q^0, while the turbulent attractor is shown by a red marker. Between the red and the blue markers, there is always a white dot with two arrows that shows a linearly unstable point of the potential $V(q)$.

overview of the model). The nonlinear dynamics of the finite-amplitude perturbation will, therefore, be determined by the transfer of kinetic energy from the laminar regions to the turbulent ones potentially leading to slugs (see the bottom panel of Fig. 2) and vice versa for decaying finite-amplitude perturbations that relax the system to the linearly stable laminar Hagen–Poiseuille state q^0 (see the top panel of Fig. 2). The critical case for which a puff is sustained without growing neither decaying is termed edge state (see the middle panel of Fig. 2).

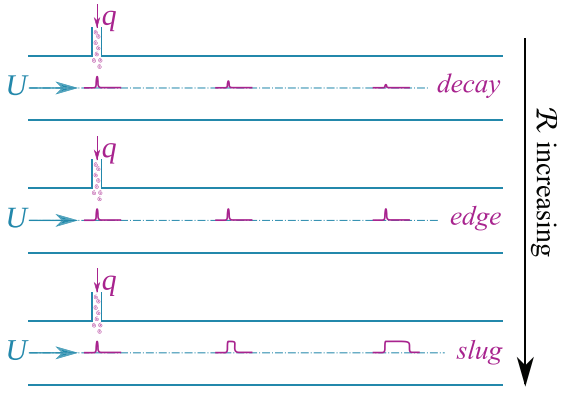

FIG. 2. Schematics of the considered transition problem. A finite-amplitude perturbation q (magenta) is injected in a pipe with average background flow velocity U (light-blue). For low-enough Reynolds numbers, small finite-amplitude perturbations decay, and the background flow remains laminar (top figure). Upon an increase in the Reynolds number, the background flow can transfer energy to the finite-amplitude perturbation q, leading to a slug perturbation (bottom figure). When the Reynolds number is critical to small finite-amplitude perturbations, the edge state is recovered and q neither grows nor decays (middle figure).

Moreover, starting with the pioneering work by Scheele and Greene,[9] laminar-to-turbulent transition in simple pipes has been considered for nonisothermal flows. More recent studies focused on the effect of (i) the curvature parameter for annular pipes,[10] (ii) the inclination angle for annular and simple pipes, hence the buoyancy forces opposing the pressure gradient that drives the flow,[11] and (iii) the suppression of turbulence for heated vertical pipe flows.[12]

Building upon the model of Barkley, we propose a novel generalization of such a reduced-order approach by adding the energy equation and the thermal effect on the dynamic viscosity. We aim, therefore, at investigating the impact of temperature variations on the local and average Reynolds number considering either uniformly or differentially heated pipe walls for horizontal pipes. Finally, as observed by Bahrani and Nouar,[13] the effect of shear-thinning on the dynamics of turbulent slugs is significant. Hence, a further generalization of the model of Barkley is proposed considering a power-law fluid. To generalize the constitutive equation of the stress tensor, we consider the power-law model, i.e., $\tau = K|\dot{\gamma}|^n$, where τ and $\dot{\gamma}$ are the shear stress and the shear rate, respectively, K is the consistency index, and n denotes the power-law index. Upon a variation of the flow index n, we will then investigate shear-thinning ($n<1$) and shear-thickening ($n>1$) fluids.

Building on the model of Barkley,[6] we generalize it by including the effects of nonisothermal conditions on the dynamic viscosity $\mu(T)$ and the density $\rho(T)$ of the fluid. We consider the normalized Reynolds number $\mathcal{R}$ intended as a control parameter for the dynamics of a turbulent perturbation surrounded by the pipe mean flow $\bar{U}$. The impact of temperature on $\mathcal{R}$ is included in the model equation for the turbulent kinetic energy q,

$$\frac{\partial q}{\partial t} + (u-\zeta)\frac{\partial q}{\partial x} = q\{\mathcal{R}(T) + (u-U_0) - [\mathcal{R}(T)+\delta](q-1)^2\} + D\frac{\partial^2 q}{\partial x^2}, \quad (1)$$

where t and x denote the time and space coordinate (along the pipe axis), respectively, T and u are the centerline temperature and turbulent velocity, respectively, U_0 and δ are parameters that model the potential forcing of the kinetic energy; the advection velocity for a turbulent perturbation is $(u-\zeta)$, where ζ is another model parameter and D is a diffusion coefficient included to characterize the dynamics of q by means of a nonlinear reaction-advection–diffusion equation.

In terms of the centerline turbulent velocity, our generalization to the model of Barkley[6] reads

$$\frac{\partial u}{\partial t} + (U_0+c)\frac{\partial u}{\partial x} = \epsilon_1(U_0-u) + \epsilon_2(\bar{U}-u)q + \frac{\mathcal{R}(\bar{T})}{\nu(\bar{T})}\frac{\partial \nu}{\partial T}\frac{\partial T}{\partial x}\frac{\partial u}{\partial x} + \mathcal{R}(T)\frac{\partial^2 u}{\partial x^2}, \quad (2)$$

where the convective velocity is (U_0+c), ϵ_1 and ϵ_2 are two model parameters related to the turbulent dissipation, $\nu(T) = \mu(T)/\rho(T)$, and $\bar{T}$ is the reference temperature. Our model includes the thermal effect on the local Reynolds number (last term of the RHS) as well as on the shear stress tensor (second last term of the RHS).

Finally, as the two equations are coupled with the temperature at the pipe centerline, the energy equation is included in the model, assuming the same convective velocity of u and including a normalized Prandtl number, $\mathcal{P}$, which is the counterpart of $\mathcal{R}$,

$$\frac{\partial T}{\partial t} + (U_0 + c)\frac{\partial T}{\partial x} = \mathcal{P}\frac{\partial^2 T}{\partial x^2} + Q_{heat}(x), \tag{3}$$

where for simplicity, $\mathcal{P}$ is assumed as a constant. The term $Q_{heat}(x)$ denotes a nonconstant heat source distributed along the pipe axis.

A second generalization of the original model consists of including non-Newtonian effects for power-law fluids in (2). It yields

$$\frac{\partial u}{\partial t} + (U_0 + c)\frac{\partial u}{\partial x} = \epsilon_1(U_0 - u) + \epsilon_2(\bar{U} - u)q + \left|\frac{\partial u}{\partial x}\right|^{n-1}\left[\frac{\mathcal{R}(\bar{T})}{\nu(\bar{T})}\frac{\partial \nu}{\partial T}\frac{\partial T}{\partial x}\frac{\partial u}{\partial x} + \mathcal{R}(T)\frac{\partial^2 u}{\partial x^2}\right], \tag{4}$$

where n is the power-law index. The other two equations of the model remain unchanged. We stress that such a generalization is consistent with the one-dimensional with of the original model of Barkley and makes use of a simplification hypothesis: only the axial stretching component of the strain-rate tensor norm is retained, i.e., $|\dot{\gamma}| = \sqrt{\vec{\vec{D}} : \vec{\vec{D}}} \approx \partial_x u$, where $\vec{\vec{D}}$ is the deformation rate tensor. This has a significant impact especially at the fronts of the perturbations, where $\partial_x u$ is high. Retaining such a non-Newtonian feature provides a leading-order effect for understanding the dynamics of puffs and slugs.

We validate the model as follows. The three-equation model is discretized by finite differences in time and space. The explicit Euler method is used, in combination with the first-order upwind scheme for the first-order derivatives, and the second-order centered scheme for the second-order derivatives, i.e.,

$$\left.\frac{\partial A}{\partial t}\right|_{(t,x)=(t^k,x_i)} \approx \frac{A_i^{k+1} - A_i^k}{t^{k+1} - t^k}, \tag{5a}$$

$$\left.\frac{\partial^2 A}{\partial x^2}\right|_{(t,x)=(t^k,x_i)} \approx \frac{A_{i+1}^k - 2A_i^k + A_{i-1}^k}{x_{i+1} - x_{i-1}}, \tag{5b}$$

$$\left.\frac{\partial A}{\partial x}\right|_{(t,x)=(t^k,x_i)} \approx \frac{A_{i+1}^k - A_i^k}{x_{i+1} - x_i}, \tag{5c}$$

$$\left. u\frac{\partial q}{\partial x}\right|_{(t,x)=(t^k,x_i)} \approx u_i^k \frac{q_{i+1}^k - q_i^k}{x_{i+1} - x_i}, \tag{5d}$$

$$\left.\frac{\partial \nu}{\partial T}\frac{\partial T}{\partial x}\frac{\partial u}{\partial x}\right|_{(t,x)=(t^k,x_i)} \approx \frac{\nu_{i+1}^k - \nu_i^k}{T_{i+1}^k - T_i^k}\frac{T_{i+1}^k - T_i^k}{x_{i+1} - x_i}\frac{u_{i+1}^k - u_i^k}{x_{i+1} - x_i}, \tag{5e}$$

where A is a placeholder that either denotes q, u, or T, the superscript k denotes the current time $t = t^k$, while the superscript i refers to the collocated node at $x = x_i$. The time step $\Delta t = t^{k+1} - t^k, \forall k$, is kept constant as well as the grid size $\Delta x = x_{i+1} - x_i, \forall i$. This same approach has been used by Barkley,[6] and a comparison with his model results (for a Newtonian isothermal flow) is presented in Fig. 3. The top figure depicts the (u, q) phase-space, while the perturbation at final time $t = 100$ is shown in the bottom panels. The marker denotes the results of Barkley,[8] while the solid lines are ours. Three normalized Reynolds numbers are considered, i.e., $\mathcal{R} = 0.6$, 0.9, and 1.8. Such three Reynolds numbers lead to two different perturbation shapes (*puff* for $\mathcal{R} = 0.6$ and slug for $\mathcal{R} = 0.9$ and 1.8), and they relate to two qualitatively different potentials, i.e., the laminar state is the dominant attractor for $\mathcal{R} = 0.6$ and $\mathcal{R} = 0.9$, while the turbulent state becomes the strongest attractor for $\mathcal{R} = 1.8$. The satisfactory comparison with literature results concludes the validation of our solver.

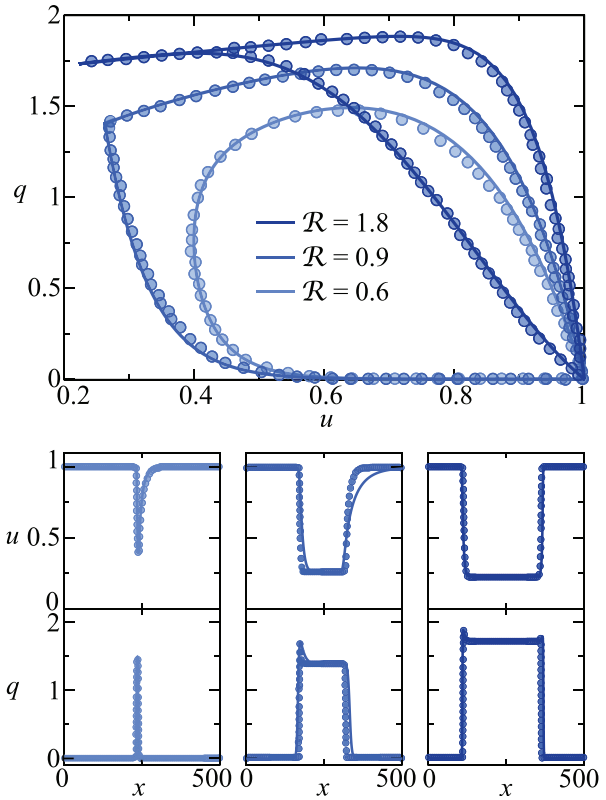

FIG. 3. Validation of our numerical model (lines) with the literature results for a Newtonian isothermal flow (markers).[8] Three normalized Reynolds numbers are considered, i.e., $\mathcal{R} = 0.6$, 0.9, and 1.8, and the comparison is carried out in the (u, q) phase-space (top figure) and in terms of the final shape of the perturbation (bottom panels).

As the effect of temperature is considered on the thermophysical properties, we assumed that the fluid flowing in the pipe is water, hence,

$$\mu(T) = 2.414 \times 10^{-5} \times 10^{247.8/(T[K]-140)}, \tag{6a}$$

$$\rho(T) = \rho(\bar{T}) + \beta(T - \bar{T}), \tag{6b}$$

where $T[K]$ is the dimensional temperature in kelvin, and a linear approximation of the water density variation is considered for simplicity, with β being the corresponding thermal expansion factor. Within the framework of our model, the term $Q_{heat}(x)$ in Eq. (3) is used to include heat sources. Two heat flow configurations have been considered to investigate the effect of nonisothermal walls on the transition to turbulence.

The first case we consider models a uniformly heated pipe, i.e., we set $Q_{heat}(x) = \bar{Q}_{heat}$. The constant heat source intensity applied all over the pipe wall $\bar{Q}_{heat}$ is assumed as parameter of our first investigation, together with the reduced Reynolds number at reference temperature, $\mathcal{R}(\bar{T})$. The reduced Prandtl number at reference temperature,

$\mathcal{P}(\bar{T})$, is kept constant to $\mathcal{P}(\bar{T}) = 1$, and the other parameters are set as in previous works that employ the model of Barkley, see Table I. Periodic boundary conditions are applied, and the length of the pipe domain always equals $L = 1000$ in our simulations, i.e., $x \in [0, L]$. As initial conditions, we set the reference values for temperature $T(t = 0) = 1$ and velocity $u(t = 0) = 1$ at start, while q is initiated as a square wave of amplitude $q_{\max}(t = 0) = 0.5$ between $x = 1$ and $x = 3$ and zero everywhere else. Figure 4 depicts the phase diagram of a fully developed initially small perturbation for three reference Reynolds numbers, i.e., $\mathcal{R}(\bar{T}) = 0.6$, 0.9, and 1.3, corresponding to the three panels of the figure. In each panel, the effect of six constant heat sources is considered within the range $\bar{Q}_{heat} \in [0, 0.05]$. Uniformly heating the horizontal pipe always destabilizes the flow playing in favor of transition to turbulence. This is especially evident for $\mathcal{R}(\bar{T}) = 0.6$, where a small perturbation decays for $\bar{Q}_{heat} = 0$ (see gray marker, leading to the laminar state q^0), whereas even a weak uniform heat source, $\bar{Q}_{heat} = 0.01$, changes the character of the pipe flow leading the same initially small perturbation to grow. The reported destabilization is an interplay of two main effects: (i) an increase in the average temperature leads to an increase in the average Reynolds number and (ii) owing to the differential effects of the temperature gradient along the pipe axis, the convective effects of transport are reduced. Within the model framework, the first effect is related to the factor $\mathcal{R}(\bar{T})$ present in (1) and (2), while the latter effect is rather induced by the second last term of the right-hand side of (2), which brought on the left-hand side leads to an effective convective velocity $U_{conv} = U_0 + c - \mathcal{R}(\bar{T})\partial_T \nu \partial_x T/\nu(\bar{T})$. The increase in the average Reynolds number $\langle \mathcal{R}(T) \rangle$ over the reference Reynolds number $\mathcal{R}(\bar{T})$ is a destabilizing effect; on the other hand, the effect of the kinematic viscosity rate of change with the temperature is more complex. As $\partial_T \nu < 0$, the effective convective velocity U_{conv} increases. To isolate the effect of an enhanced convective velocity, we compute the $(u, q)-$phase diagram for $c = 1$ and $c = 1.5$ and remove thermal effects (not shown). Upon an increase in the convective velocity, a higher turbulent kinetic energy is observed for $u \gtrapprox 0.55$. On the other hand, when $u \lessapprox 0.55$, q is larger for perturbations transported at a slower convective velocity.

This same trend is further confirmed by the results presented in Fig. 5, where a linear heat source is considered, i.e., $Q_{heat}(x)p = \Delta Q_{heat}(2x/L - 1)$, where L is the pipe length and ΔQ_{heat} is the amplitude of cooling and heating at $x = 0$ and $x = L$, respectively. The differential heat load considered has, therefore, average equal to zero, hence no net energy is injected into the system. This leads to an average Reynolds number almost equal to the reference Reynolds number $\langle \mathcal{R}(T) \rangle \approx \mathcal{R}(\bar{T})$. The difference among the two of them is only due to the convective effect of (3) on the temperature, hence to the derivative of the kinematic viscosity with respect to T. As depicted in Fig. 5, upon an increase in ΔQ_{heat}, the turbulent kinetic energy increases at high velocities u, and it decreases at lower velocities. The net effect on the flow is that the turbulent perturbation is narrower, faster, and locally more energetic when ΔQ_{heat} is increased. This leads to a nontrivial stabilizing effect quantified by the shrinkage of the phase diagram (u, q), such that for $\Delta Q_{heat} \geq 4$, the turbulent perturbation decays even for $\mathcal{R}(\bar{T}) = 0.9$.

In order to relate our model parameters to actual heat loads, we identify the range of dimensional parameters our study applies to.

TABLE I. Summary of the model parameters employed for all the results of this study.

δ	ϵ_1	ϵ_2	ζ	U_0	c	D	$\bar{T}$ (K)	$\rho(\bar{T})$ (g/cm^3)	β
0.1	0.04	0.2	0.8	1	1	1	298	1000	0.0002

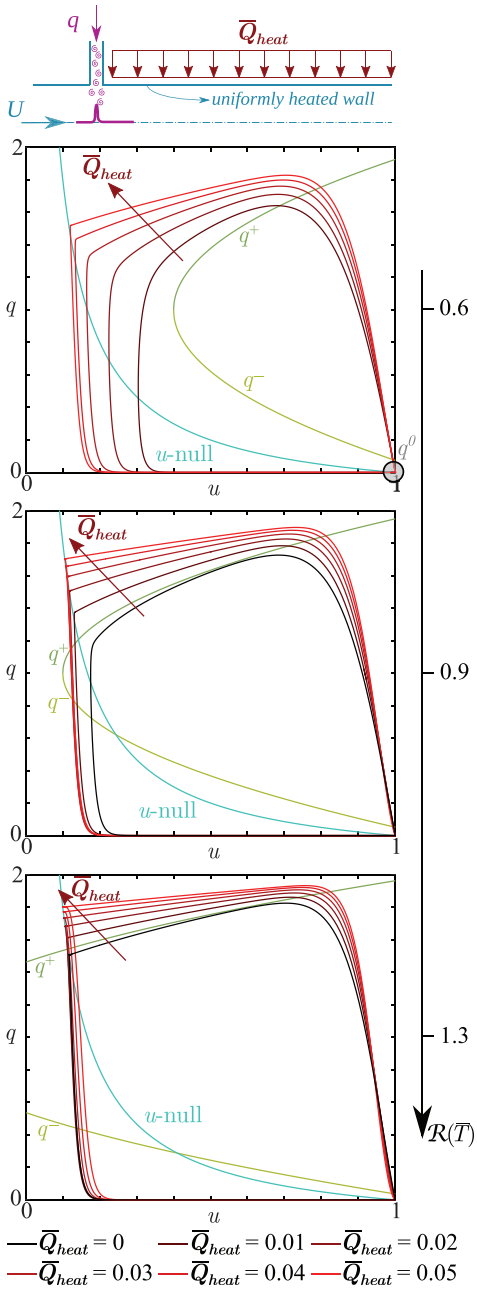

FIG. 4. Dynamics of the perturbation in the (u, q)-phase space for $\mathcal{R} = 0.6$, 0.9, and 1.3 and $\bar{Q}_{heat} \in [0, 0.05]$. The (u, q)-phase diagrams are colored from black to light-red, i.e., from the weakest ($\bar{Q}_{heat} = 0$) to the strongest uniform heat load ($\bar{Q}_{heat} = 0.05$).

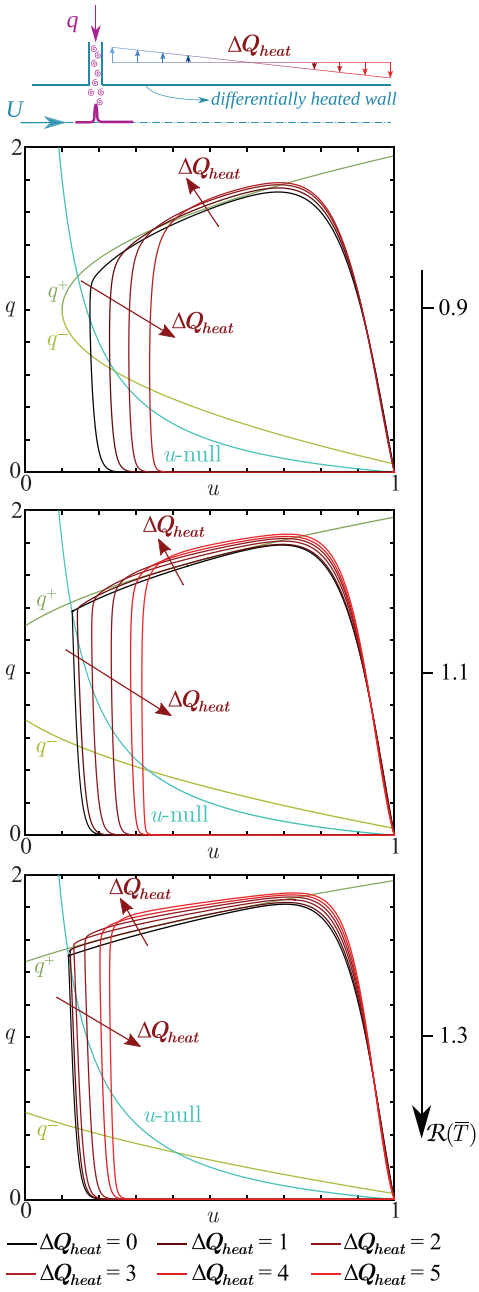

FIG. 5. Dynamics of the perturbation in the (u, q)-phase space for $\mathcal{R} = 0.9$, 1.1, and 1.3 and $\Delta Q_{heat} \in [0, 5]$. The (u, q)-phase diagrams are colored from black to light-red, i.e., from the weakest ($\Delta Q_{heat} = 0$) to the strongest differential heat load ($\Delta Q_{heat} = 5$).

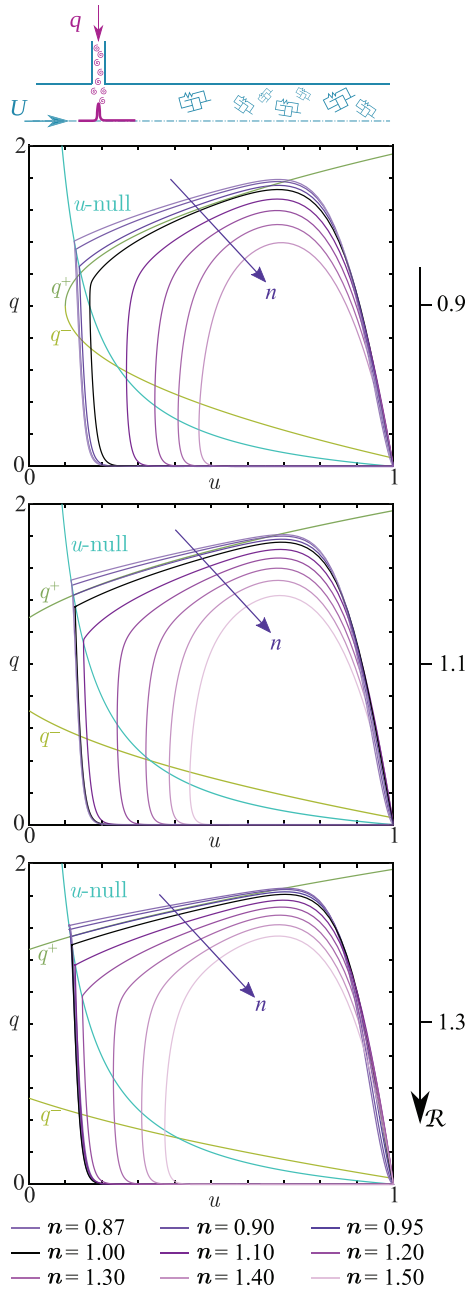

FIG. 6. Dynamics of the perturbation in the (u, q)-phase space for $\mathcal{R} = 0.9$, 1.1, and 1.3 and $n \in [0.85, 1.5]$. The (u, q)-phase diagrams are colored from black to light-purple for increasingly shear-thinning fluids ($n \leq 1$, with black for $n = 1$, i.e., Newtonian) and from black to light-magenta for increasingly shear-thickening fluids ($n \geq 1$, with black for $n = 1$, i.e., Newtonian).

As we consider water, i.e., $\nu(T = 298\,\mathrm{K}) = 8.93 \times 10^{-6}$ Pa s, and $\mathcal{R} \in [0.6, 1.3]$, i.e., $\mathrm{Re} = \bar{U}D/\nu \in [1380, 2990]$, the product of $\bar{U}$ and D must be within the range $\bar{U}D \in [0.0123, 0.0267]$ m^2/s. Since $\bar{Q}_{\mathrm{heat}} \in [0, 0.05]$, i.e., $\bar{U}/D \in [0, 14.9]$ s^{-1}, that leads to minimum pipe diameters $D \in [0.0287, 0.0423]$ m for the hottest uniform heat load. Similar considerations apply to the differential heat load, for which we find minimum pipe diameters $D \in [0.002\,87,\ 0.004\,23]$ m. Hence, our heat load parameters apply to pipe diameters larger than 0.0287 m for uniform heat loads and to diameters larger than 0.002 87 m for differential heat loads.

Finally, the third thermally related parameter considered in our study is the normalized Prandtl number $\mathcal{P}$. We find that, for a horizontal differentially heated pipe with $\Delta Q_{heat} = 1$, upon a variation of the normalized Prandtl number within the range $\mathcal{P} \in [0.1, 5]$, a negligible effect on the perturbation dynamics is observed. For figures plotted with the same layout of Fig. 5, no significant difference between the curves corresponding to $\mathcal{P} \in [0.1, 5]$ is observed in the (u, q)-phase space. We, therefore, conclude that the stabilizing/destabilizing effects due to differential/constant heating do not depend significantly on the diffusion term of the energy equation. Hence, our results are robust with respect to the considered fluid. This, therefore, confirms that the simplifying hypothesis of constant Prandtl number $\mathcal{P}$ done in (3) is reliable.

The last generalization of our study consists of including non-Newtonian effects by assuming a power-law fluid inside the pipe. In this case, the power-law index n is taken as control parameter, and no thermal effects are considered. Figure 6 depicts the impact of n on the perturbation in the (u, q)-phase space for shear-thinning ($n < 1$, i.e., $n = 0.87$, 0.9, and 0.95) and shear-thickening ($n > 1$, i.e., $n = 1.1$, 1.2, 1.3, 1.4, and 1.5) fluids. A consistent trend is demonstrated upon an increase in the power-law index n, leading to a stabilization of the finite-size amplitude perturbation by a corresponding reduction of the area of the perturbation diagram. This same trend is preserved upon an increase in the normalized Reynolds number. For understanding this effect, we can refer to the impact of the power-law index on the deformation rate, i.e., to $|\partial_x u|^{n-1}$. This term has a net effect on the flow as it multiplies the normalized Reynolds number. When $n < 1$, the average of $|\partial_x u|^{n-1}$ is larger than 1; hence, the effective Reynolds number given by $\mathcal{R}_{\text{eff}} = \overline{|\partial_x u|^{n-1}}\mathcal{R}$ increases. On the other hand, when $n > 1$, the average of $|\partial_x u|^{n-1}$ is smaller than 1, and the perturbation gets stabilized as $\mathcal{R}_{\text{eff}}$ decreases.

A generalization of the model of Barkley[6] has been proposed to study the effect of thermal loads and non-Newtonian (power-law) constitutive laws on the transition to turbulence in pipe flows. Two thermal loads have been considered, i.e., a uniformly ($\bar{Q}_{heat}$) and a differentially (ΔQ_{heat}) heated wall. For uniformly heated walls, a net destabilization effect (i.e., a transition to turbulence for lower reference Reynolds numbers) is demonstrated for all the considered parameters, and it is mainly due to an increase in the average Reynolds number. This is consistent with the experimental results by Everts and Meyer,[14] who consider a horizontal pipe flow and found that increasing the constant heat flux applied to the pipe wall shifts the laminar-to-turbulence transition to lower Reynolds numbers. On the other hand, for differentially heated walls, the convective effect related to the spatial variation of the local Reynolds number led to higher levels of turbulent intensity for slower perturbations when increasing ΔQ_{heat}. As a result, we found this convective term to represent a nontrivial stabilizing effect. Moreover, considering power-law fluids, we found that a clear stabilization is induced by an increase in the power-law index n. This means that by increasing the degree of shear thinning ($n \downarrow$ for $n < 1$), the system tends to destabilize, while increasing the shear thickening ($n \uparrow$ for $n > 1$), the pipe flow becomes more stable. A last consideration is dedicated to the impact of our generalized model, as it proposes a simplified framework for predicting potential stabilization/destabilization trends. We, therefore, expect that our generalized model could serve to test heat control protocols applied to Newtonian and non-Newtonian pipe flows.

DATA AVAILABILITY

The data that support the findings of this study are available from the corresponding author upon reasonable request.

REFERENCES

[1] F. Romanò, "Stability of generalized Kolmogorov flow in a channel," Phys. Fluids **33**, 024106 (2021).
[2] G. Lemoult, L. Shi, K. Avila, S. V. Jalikop, M. Avila, and B. Hof, "Directed percolation phase transition to sustained turbulence in Couette flow," Nat. Phys. **12**, 254–258 (2016).
[3] X. Zhu, V. Mathai, R. J. A. M. Stevens, R. Verzicco, and D. Lohse, "Transition to the ultimate regime in two-dimensional Rayleigh-Bénard convection," Phys. Rev. Lett. **120**, 144502 (2018).
[4] B. Hof, C. W. H. Van Doorne, J. Westerweel, F. T. M. Nieuwstadt, H. Faisst, B. Eckhardt, H. Wedin, R. R. Kerswell, and F. Waleffe, "Experimental observations of nonlinear traveling waves in turbulent pipe flow," Science **305**, 1594–1598 (2004).
[5] F. Waleffe, "On a self-sustaining process in shear flows," Phys. Fluids **9**, 883–900 (1997).
[6] D. Barkley, "Simplifying the complexity of pipe flow," Phys. Rev. E **84**, 016309 (2011).
[7] D. Barkley, B. Song, V. Mukund, G. Lemoult, M. Avila, and B. Hof, "The rise of fully turbulent flow," Nature **526**(7574), 550–553 (2015).
[8] D. Barkley, "Theoretical perspective on the route to turbulence in a pipe," J. Fluid Mech. **803**, P1 (2016).
[9] G. F. Scheele and H. L. Greene, "Laminar-Turbulent transition for nonisothermal pipe flow," AIChE J. **12**(4), 737–740 (1966).
[10] A. Khan, P. Bera, and M. K. Khandelwal, "Bifurcation and instability of annular Poiseuille flow in the presence of stable thermal stratification: Dependence on curvature parameter," Phys. Fluids **31**(10), 104105 (2019).
[11] G. Saha and M. C. Paul, "Transition of nanofluids flow in an inclined heated pipe," Int. Commun. Heat Mass Transfer **82**, 49–62 (2017).
[12] E. Marensi, S. He, and A. P. Willis, "Suppression of turbulence and travelling waves in a vertical heated pipe," J. Fluid Mech. **919**, A17 (2021).
[13] S. A. Bahrani and C. Nouar, "Intermittency in the transition to turbulence for a shear-thinning fluid in Hagen-Poiseuille flow," J. Appl. Fluid Mech. **7**, 1–6 (2014).
[14] M. Everts and J. P. Meyer, "Heat transfer of developing and fully developed flow in smooth horizontal tubes in the transitional flow regime," Int. J. Heat Mass Transfer **117**, 1331–1351 (2018).